Cerebral Cortex, August 2016;26: 3413–3427

doi:10.1093/cercor/bhv172
Advance Access Publication Date: 28 July 2015
Original Article

ORIGINAL ARTICLE

Resting-State Functional Connectivity of the Locus Coeruleus in Humans: In Comparison with the Ventral Tegmental Area/Substantia Nigra Pars Compacta and the Effects of Age

Sheng Zhang[1], Sien Hu[1], Herta H. Chao[2,3], and Chiang-Shan R. Li[1,4,5,6]

[1]Department of Psychiatry, [2]Department of Internal Medicine, Yale University, New Haven, CT 06519, USA, [3]Medical Service, VA Connecticut Health Care System, West Haven, CT 06516, USA, [4]Department of Neurobiology, [5]Interdepartmental Neuroscience Program, Yale University, New Haven, CT 06520, USA, and [6]Connecticut Mental Health Center, New Haven, CT 06519, USA

Address correspondence to Dr Chiang-Shan Ray Li, Connecticut Mental Health Center S112, 34 Park Street, New Haven, CT 06519, USA.
Email: chiang-shan.li@yale.edu

Abstract

The locus coeruleus (LC) provides the primary noradrenergic inputs to the cerebral cortex. Despite numerous animal studies documenting the functions of the LC, research in humans is hampered by the small volume of this midbrain nucleus. Here, we took advantage of a probabilistic template, explored the cerebral functional connectivity of the LC with resting-state fMRI data of 250 healthy adults, and verified the findings by accounting for physiological noise in another data set. In addition, we contrasted connectivities of the LC and the ventral tegmental area/substantia nigra pars compacta. The results highlighted both shared and distinct connectivity of these 2 midbrain structures, as well as an opposite pattern of connectivity to bilateral amygdala, pulvinar, and right anterior insula. Additionally, LC connectivity to the fronto-parietal cortex and the cerebellum increases with age and connectivity to the visual cortex decreases with age. These findings may facilitate studies of the role of the LC in arousal, saliency responses and cognitive motor control and in the behavioral and cognitive manifestations during healthy and disordered aging. Although the first to demonstrate whole-brain LC connectivity, these findings need to be confirmed with high-resolution imaging.

Key words: dopamine, locus ceruleus, noradrenaline, resting-state functional connectivity, VTA

Introduction

Cognitive functions, such as working memory, attention, and executive control, are influenced by catecholamines [Harley 1991; Coull et al. 1999; Aston-Jones and Cohen 2005; Arnsten 2007; Minzenberg et al. 2008; Kahnt and Tobler 2013; Clewett et al. 2014; see also Bari and Robbins (2013), Li (2013), Clark and Noudoost (2014), and Rubia et al. (2014) for a review]. Midbrain dopaminergic (DA) neurons in the ventral tegmental area/substantia nigra pars compacta (VTA/SNc) and noradrenergic (NA) neurons in the locus coeruleus (LC) are major sources of these influences. NA and DA systems are both involved in motivated behaviors (Chandler, Waterhouse, et al. 2014, for a review); while pharmacological studies described the influence of NA and DA manipulations on cognitive and affective functioning, it is not clear how LC and VTA/SNc contribute to these processes by interacting with other brain regions.

There is evidence for diverse rather than homogeneous cerebral projections of the 2 systems (Chandler, Waterhouse, et al. 2014), with important etiology and treatment implication for mental disorders (Arnsten and Li 2005; Del Campo et al. 2011; Bari and Robbins 2013; Hamon and Blier 2013). DA and NA signaling may be involved in functionally opposing processes. For instance, aversive stimuli activated NA but inhibited DA signaling, whereas palatable stimuli inhibited norepinephrine while causing dopamine release, in the bed nucleus of stria terminalis (Park et al. 2012). On the other hand, the NA and DA systems interact functionally. Studies have provided evidence supporting LC regulation of DA processes. Extracellular dopamine in the cerebral cortex originates not only from DA but also from NA terminals [see Devoto and Flore (2006) for a review], and synaptic dopamine is captured by both norepinephrine and dopamine transporters (Bymaster et al. 2002; Carboni et al. 2006). Dopamine binds to alpha-2 adrenergic receptors albeit with lower affinity (Cornil and Ball 2008). Both dopamine and norepinephrine bind to dopamine D4 receptors, which may be activated at least in part through volume transmission, as suggested by a mismatch between D4 and tyrosine hydroxylase/dopamine beta-hydroxylase immunoreactivity (Rivera et al. 2008). Chemical modulation or electrical stimulation of the LC alters both norepinephrine and dopamine concentration in the cerebral cortex, and NA fibers may be the primary source of a DA-mediated increase in synaptic transmission in the hippocampus (Smith and Greene 2012). LC may contribute to DA transmission under physiological conditions and in response to antidepressants and drugs of abuse. Taken together, these studies suggest neurobiological bases for both shared and distinct roles of the NA and DA systems in a wide range of cerebral processes.

Analysis of resting-state fMRI data has proved to be a useful approach to characterizing functional architecture of a brain region. Specifically, low-frequency blood oxygenation level-dependent (BOLD) signal fluctuations reflect connectivity between functionally related brain regions (Biswal et al. 1995; Fair et al. 2007; Fox and Raichle 2007). For instance, based on correlation in spontaneous BOLD activity, investigators have used various clustering algorithms to identify voxels of similar connectivity and describe functional subdivisions of the thalamus (Zhang et al. 2008, 2010), basal ganglia (Barnes et al. 2010), medial superior frontal cortex (Kim et al. 2010; Zhang et al. 2012), anterior cingulate cortex (ACC; Margulies et al. 2007), orbitofrontal cortex (Kahnt et al. 2012), cerebellum (O'Reilly et al. 2010), and precuneus (Margulies et al. 2009; Cauda et al. 2010; Zhang and Li 2012a).

Recently, Tomasi and Volkow (2014) characterized functional connectivity of the VTA/SNc in adolescents and young adults. Both the VTA and SNc demonstrated bilateral positive connectivity with the globus pallidus, cerebellar vermis, and ACC, and negative connectivity with the occipital cortex. The transition from adolescence to young adulthood is marked by increased connectivity to limbic regions and default mode network and by decreased connectivity to motor and medial temporal cortices. Murty et al. (2014) employed manually drawn masks and showed greater SNc connectivity to the dorsomedial prefrontal cortex, somatomotor cortex, superior temporal gyrus, and inferior parietal lobule, and greater VTA connectivity to the nucleus accumbens, hippocampus, cerebellum, and posterior midbrain. However, to our knowledge, no studies have described whole-brain functional connectivity of the LC during resting state.

The current study aimed to employ a probabilistic map of LC recently developed by Keren et al. (2009) and characterize whole-brain functional connectivity of the LC, as a step to understanding the systems-level connectivity of this midbrain structure in humans. In particular, we compared the functional connectivities of LC and VTA/SNc in the hope to delineate the shared and distinct circuits of these 2 structures and further our understanding of the interacting roles of LC and VTA/SNc in health and illness. Additional goals were to explore the effects of age on the functional connectivities of the LC and VTA/SNc. Aging is associated with changes in catecholamine levels in the brain (Goldman-Rakic and Brown 1981; Wenk et al. 1989). While the VTA/SNc is known to demonstrate age-related degeneration (Huang et al. 1995; Yoshimoto et al. 1998; Dreher et al. 2008), less is understood of age-related changes in the LC. Thus, examining age-dependent patterns of LC connectivity may facilitate research of the neural bases of mild cognitive impairment, Alzheimer's disease, and other degenerative disorders that implicate NA systems.

Although this study is exploratory, we had a few hypotheses in place. First, as there is shared synaptic action and regulation of dopamine and norepinephrine, as described above, we posited that LC and VTA/SNc would demonstrate connectivity overlapping across multiple brain regions. Second, we posited a more significant LC than VTA/SNc connectivity to the thalamus, amygdala, and brain stem, which are implicated in LC-mediated arousal (Macefield et al. 2013; Colavito et al. 2015) and contain high density of norepinephrine transporter (NET; Wilson et al. 2003; Smith and Porrino 2008), dopamine-β-hydroxylase, an enzyme that converts dopamine to norepinephrine (Agarwal et al. 1993; Ginsberg et al. 1993; Baldo et al. 2003), as well as norepinephrine and its metabolites (Fahn et al. 1971; Moses and Robins 1975; Mackay et al. 1978; Herregodts et al. 1991). In contrast, the basal ganglia including both ventral and dorsal striatum would demonstrate higher VTA/SNc than LC connectivity because of its heavy DA innervations (Hortnagl et al. 1983; al-Tikriti et al. 1995; Schonbachler et al. 2002). Third, there is evidence that the DA system is evolutionally more ancient than the NA system (Moret et al. 2004; Caveney et al. 2006) and the limbic regions including the parahippocampal gyrus and certain midline brain regions are phylogenetically older (Panksepp and Biven 2012). Furthermore, histochemistry showed that more VTA than LC cells are retrogradely labeled that project to the medial prefrontal cortex, orbitofrontal cortex, and ACC (Chandler et al. 2013). Thus, we posited that there would be more significant LC and VTA/SNc connectivity each to lateral and midline cerebral structures. A system-level characterization of the cerebral connectivity of LC and VTA/SNc would complement studies of pharmacological manipulations to advance research of DA and NA functions.

Materials and Methods

Resting-State Data

Resting-state fMRI scans were pooled from 3 data sets (Leiden_2180 /Leiden_2200, Newark, and Beijing_Zang, $n = 144$), downloadable from the 1000 Functional Connectomes Project (Biswal et al. 2010), and our own data ($n = 106$). In selecting the data, we tried to include as many subjects as possible in order to have more stable findings in the current study, as in our earlier work (Zhang et al. 2012; Zhang and Li 2014). We used only datasets acquired under conditions identical to our own [e.g., similar repetition time (TR), all under 3 T, all eyes closed]. Individual subjects' images were viewed one by one to ensure that the whole brain was covered. A total of 250 healthy subjects' resting-state data (18–49 years of age; 104 men; one scan per participant; duration: 4.5–10 min) were analyzed. Table 1 summarizes these data sets.

Table 1 Demographic information and imaging parameters of the resting-state functional MRI data obtained from the image repository for the 1000 Functional Connectomes Project and our laboratory

Dataset	Subjects	Ages (years)	Time points	TR (s)	Slice acquisition order
Beijing_Zang	31 M/66 F	18–26	225	2	Interleaved ascending
Leiden_2180	10 M/0 F	20–27	215	2.18	Sequential descending
Leiden_2200	11 M/8 F	18–28	215	2.2	Sequential descending
Newark	9 M/9 F	21–39	135	2	Interleaved ascending
Our own	63 M/43 F	19–49	295	2	Interleaved ascending

M: males; F: females; TR: repetition time.

Imaging Data Preprocessing

Brain imaging data were preprocessed using Statistical Parametric Mapping (SPM 8, Wellcome Department of Imaging Neuroscience, University College London, UK). Images from the first 5 TRs at the beginning of each trial were discarded to enable the signal to achieve steady-state equilibrium between RF pulsing and relaxation. Standard image preprocessing was performed. Images of each individual subject were first realigned (motion corrected) and corrected for slice timing. A mean functional image volume was constructed for each subject per run from the realigned image volumes. These mean images were co-registered with the high-resolution structural image and then segmented for normalization with affine registration followed by nonlinear transformation (Friston et al. 1995; Ashburner and Friston 1999). The normalization parameters determined for the structure volume were then applied to the corresponding functional image volumes for each subject. Finally, the images were smoothed with a Gaussian kernel of 8 mm at full width at half maximum. While an 8-mm smoothing kernel is advantageous in characterizing cortical connectivity, in a separate set of analysis, we examined the connectivities of the LC and VTA/SNc using the same data smoothed with a 4-mm kernel.

Additional preprocessing was applied to reduce spurious BOLD variances that were unlikely to reflect neuronal activity (Rombouts et al. 2003; Fox et al. 2005; Fair et al. 2007; Fox and Raichle 2007). The sources of spurious variance were removed through linear regression by including the signal from the ventricular system, white matter, and whole brain, in addition to the 6 parameters obtained by rigid body head motion correction. First-order derivatives of the whole brain, ventricular, and white matter signals were also included in the regression.

Cordes et al. (2001) suggested that BOLD fluctuations below a frequency of 0.1 Hz contribute to regionally specific BOLD correlations. Thus, we applied a temporal band-pass filter ($0.009\ \text{Hz} < f < 0.08\ \text{Hz}$) to the time course in order to obtain low-frequency fluctuations, as in previous studies (Lowe et al. 1998; Fox et al. 2005; Fair et al. 2007; Fox and Raichle 2007).

Head Motion

As extensively investigated in Van Dijk et al. (2012), micro-head motion (>0.1 mm) is an important source of spurious correlations in resting-state functional connectivity analysis (Van Dijk et al. 2012). Therefore, we applied a "scrubbing" method proposed by Power et al. (2012) and successfully applied in previous studies (Smyser et al. 2010; Power et al. 2012; Tomasi and Volkow 2014) to remove time points affected by head motions. Briefly, for every time point t, we computed the "framewise displacement" given by $\text{FD}(t) = |\Delta d_x(t)| + |\Delta d_y(t)| + |\Delta d_z(t)| + r|\alpha(t)| + r|\beta(t)| + r|\gamma(t)|$, where (d_x, d_y, d_z) and (α, β, γ) are the translational and rotational movements, respectively, and r (50 mm) is a constant that approximates the mean distance between the center of Montreal Neurological Institute (MNI) space and the cortex and transforms rotations into displacements (Power et al. 2012). The second head movement metric was the root mean square variance (DVARS) of the differences in % BOLD intensity $I(t)$ between consecutive time points across brain voxels, computed as follows: $\text{DVARS}(t) = \sqrt{\langle |I(t) - I(t-1)|^2 \rangle}$, where the brackets indicate the mean across brain voxels. Finally, to compute each subject's correlation map, we removed every time point that exceeded the head motion limit $\text{FD}(t) > 0.5$ mm or $\text{DVARS}(t) > 0.5\%$ (Power et al. 2012; Tomasi and Volkow 2014). On average, 1% of the time points was removed across subjects.

Seed Regions: LC and VTA/SNc

These 2 regions of interest (ROIs) are shown in Figure 1. We used a probabilistic template of the LC derived by Keren et al. (2009). The LC seed region represents the extent of peak LC signal distribution, obtained from a sample of 44 healthy adults (age range: 19–79 years) using high-resolution T_1-weighted Turbo Spin Echo (T_1-TSE) MRI, and has a volume of 93 mm^3. The T_1-TSE LC signals were likely influenced by the ferrous neuromelanin metabolites within LC neurons (Sasaki et al. 2006) and observed in sections corresponding to the greatest concentrations of LC cells in postmortem studies (German et al. 1988). The VTA/SNc region was derived from the structural MRIs of 30 healthy adults; after spatial normalization and averaging across subjects, the size of the bilateral mask was 1106 mm^3 (Ahsan et al. 2007).

Because these seeds are located in the brain stem and, in particular, the LC is adjacent to the fourth ventricle, BOLD signals in these regions can be confounded by physiological noise. We thus examined the effect of physiological noise in a Nathan Kline Institute (NKI)/Rockland sample (Nooner et al. 2012) of resting-state fMRI images of 20 healthy volunteers (23–41 years of age; 10 men; one scan per participant; duration: 5 min, gradient-echo EPI pulse sequence, TR = 2.5 s, echo time = 30 ms, flip angle = 80°, voxel size = 3.0 × 3.0 × 3.0 mm, 38 axial slices in 3.0 mm thickness covering the entire brain) of the 1000 Functional Connectomes Project (http://www.nitrc.org/projects/fcon_1000/). In this sample, cardiac and respiratory signals were continuously recorded during resting-state fMRI. Data underwent identical preprocessing including smoothing with an 8-mm Gaussian kernel, as described in the section "Imaging Data Preprocessing", so the results could be compared. An SPM toolbox (DRIFTER, http://becs.aalto.fi/en/research/bayes/drifter/) was applied to remove the physiological noises. Briefly, a model-based Bayesian method was used for retrospective elimination of physiological noise from fMRI data (Sarkka et al. 2012). The frequency trajectories of the physiological signals were first estimated by the interacting

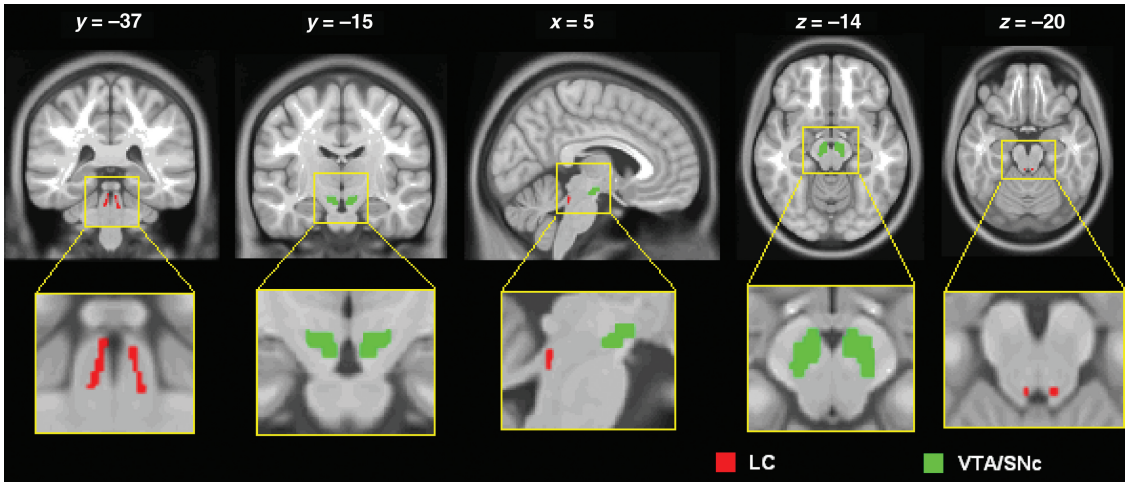

Figure 1. Seed regions: LC (red) and VTA/SNc (green), shown on axial ($z = -14$ and -20), sagittal ($x = 5$), and coronal ($y = -37$ and -15) sections. The inset shows a "blown-up" image of the location of the LC and VTA/SNc in relation to the ventricles.

multiple models filter algorithm. In a state-space model in combination of a Kalman filter and Rauch-Tung-Striebel smoother BOLD time courses were then separated into a cleaned activation-related signal, physiological noise, and white noise. Finally, the cleaned fMRI data were used to extract whole-brain correlation maps of the LC.

Seed Region-Based Linear Correlation and Random-Effects Analysis

The BOLD time courses were averaged spatially over each of the 2 seeds. For individual subjects, we computed the correlation coefficient between the averaged time course of each seed region and the time courses of all other brain voxels. To assess and compare the resting-state functional connectivity, we converted these image maps, which were not normally distributed, to z score maps by Fisher's z transform (Jenkins and Watts 1968; Berry and Mielke 2000): $z = 0.5\log_e[(1+r)/(1-r)]$. The Z maps were used in group random-effects analyses. We performed one-sample *t*-test each on the Z maps of LC and VTA/SNc and paired-sample *t*-test comparing the 2 Z maps.

Shared Cerebral Connectivity Between the LC and VTA/SNc

We identified cerebral connectivity shared between the LC and VTA/SNc, and used MarsBaR (http://marsbar.sourceforge.net/) to extract the effect size (z score) of connectivity for individual subjects. First, ROIs were identified each for positive and negative connectivities—each termed "positive ROIs" and "negative ROIs" for convenience—to LC and VTA/SNc (one-sample *t*-test, $P < 0.05$, corrected for familywise error of multiple comparisons). Shared brain regions were then identified by a logical "AND" between "positive ROIs" of LC and VTA/SNc, between "negative ROIs" of LC and VTA/SNc, as well as between "positive ROIs" of LC and "negative ROIs" of VTA/SNc, and between "negative ROIs" of LC and "positive ROIs" of VTA/SNc.

To examine whether LC and VTA/SN connectivity to each of the shared ROIs are correlated across subjects, we performed a linear regression between the effect size of connectivity for each of the ROIs with shared LC and VTA/SNc connectivity. That is, pairwise linear regressions were performed between correlation z scores each of the LC and VTA/SNc to these ROIs. Because some of the ROIs were large and encompassed more than one region, we combined these ROIs with anatomical masks from the MNI template (Tzourio-Mazoyer et al. 2002) to define distinct regions. We reported only findings significant at $P < 0.05$ corrected for multiple comparisons (see Results).

Age-Dependent Changes and Gender Differences in LC and VTA/SNc Connectivity

We performed a simple regression of the Z maps against age, each for the LC and VTA/SNc, to identify age-related changes of functional connectivity in the 2 structures. To examine gender differences, we compared men and women with age as a covariate in an analysis of variance, each for the LC and VTA/SNc. Again, all results were reported for a corrected threshold.

Results

Whole-Brain Functional Connectivity of the LC and VTA/SNc

For each seed region, we performed one-sample *t*-test of the Z maps across the group ($n = 250$; Fig. 2*A*,*B*).

The results showed positive LC connectivity to bilateral superior frontal gyrus, primary motor cortex, inferior parietal cortex, inferior temporal cortex, anterior parahippocampual gyrus, posterior insula, putamen, pallidum, ventrolateral thalamus, midbrain, and large areas of the cerebellum. LC showed negative connectivity to a large region of bilateral visual cortex, middle/superior temporal cortex, precuneus, retrosplenial cortex, posterior parahippocampual gyrus, frontopolar cortex, caudate nucleus, as well as dorsal and medial thalamus (Fig. 2*A*).

The VTA/SNc showed positive connectivity with the dorsomedial prefrontal cortex including the supplementary motor area (SMA), pre-SMA, and dorsal ACC, as well as the rostral, perigenual, and subgenual ACC, ventrolateral/posterior thalamus including the pulvinar, ventral striatum, putamen, pallidum, insula, posterior cingulate cortex, anterior parahippocampal gyrus, inferior temporal cortex and temporal pole, midbrain, and large areas of the cerebellum. The VTA/SNc showed negative connectivity with bilateral visual cortex, posterior parietal cortex, precuneus, posterior parahippocampal gyrus, precentral cortex,

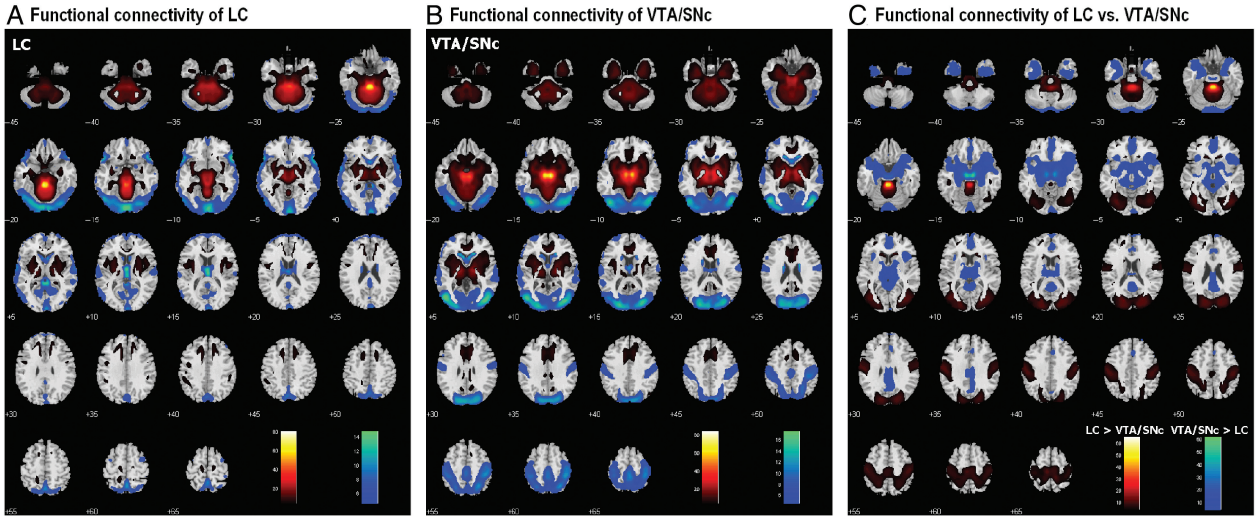

Figure 2. (*A*) Brain areas that show positive (warm color) and negative (cool color) functional connectivity to the LC; one-sample *t*-test, $P < 0.05$, corrected for familywise error of multiple comparisons. (*B*) Brain areas that show positive (warm color) and negative (cool color) functional connectivity to the VTA/SNc; one-sample *t*-test, $P < 0.05$, corrected for familywise error of multiple comparisons. (*C*) Brain areas that show differences in functional connectivity to the LC and VTA/SNc: LC > VTA/SNc (warm color); VTA/SNc > LC (cool color); paired *t*-test, $P < 0.05$, corrected for familywise error of multiple comparisons.

Table 2 Regions showing greater connectivity with LC when compared with VTA/SNc; paired *t*-test, $n = 250$

Volume (mm^3)	Peak voxel (Z)	MNI coordinate			Side	Identified brain region	Connectivity	
		x	y	z			LC	VTA/SNc
47 115	Inf	−3	−37	−23	L	Cerebellum (midline structures)	++	+
215 865	Inf	−33	−76	−2	L	Middle occipital gyrus	−	−−
	Inf	24	−82	16	R	Middle occipital gyrus	−	− −
	Inf	18	−79	22	R	Cuneus/parietal/somatomotor cortices	−/∼	− −/−
4455	Inf	18	20	16	R	Caudate head	−	− −
4131	7.20	−24	44	−8	L	Orbitofrontal/anterior middle frontal gyri	∼	−
783	7.03	−45	−34	−14	L	Middle/inferior temporal gyri	+	∼

Inf: infinity; R: right; L: left; +/−: positive and negative connectivity (with ++/− − for stronger connectivity); ∼: no significant connectivity at one-sample *t*-test, $P < 0.05$, FWE-corrected.

middle/superior temporal cortex, frontopolar cortex, dorsomedial thalamus, and caudate head (Fig. 2*B*). These results replicated previous findings of resting-state VTA/SNc connectivity with thalamus, ACC, insula, pallidum, vermis, as well as occipital cortex (Gu et al. 2010; Hadley et al. 2014; Murty et al. 2014; Tomasi and Volkow 2014).

We performed a paired *t*-test to compare functional connectivity of the LC and VTA/SNc (Fig. 2*C*). Compared with the VTA/SNc, LC showed greater connectivity to the bilateral visual, parietal, and somatomotor cortex, as well as midline cerebellar structures, and less connectivity to dorsomedial prefrontal cortex, middle and posterior cingulate cortex, ventromedial prefrontal cortex, inferior temporal cortex, anterior insula, thalamus, and the midbrain. We summarize these results in Tables 2 and 3, where we further distinguish whether a contrast arises from differences in positive or negative connectivity.

As described in the Materials and Methods section, we also examined the results with a 4-mm smoothing kernel. Visual inspection of the results showed that, while, as expected, there were diminished cortical cluster sizes, the pattern of connectivity was nearly identical to the results of 8 mm kernel (Supplementary Fig. 1), in accord with our previous work (Zhang et al. 2012; Zhang and Li 2012a). Furthermore, because the LC seed was small and close to the fourth ventricle, we examined the effects of physiological noise using the NKI/Rockland sample. First, the patterns of connectivity with and without accounting for physiological noise appeared to be similar, at least for regions that show more significant connectivity to LC (Supplementary Fig. 2). Second, we examined whether or to what extent functional connectivities of the NKI/Rockland sample mirrored those of the original sample. While the difference in sample precluded a direct comparison, we computed the effect size of connectivity of the 116 ROIs of the AAL atlas for the original sample and the NKI/Rockland sample with and without the physiological noise removed. Pairwise regressions showed that the LC connectivity of these 116 ROIs was each highly correlated ($P < 2.1 \times 10^{-34}$, $r = 0.86$–0.92; Fig. 3). These results suggest that physiological noise has limited influence on LC functional connectivity, and that whole-brain connectivities of the original and NKI/Rockland samples are consistent.

Considering that the LC (93 mm^3) is much smaller than the VTA/SNc (1106 mm^3) seed, we examined whether volume size may affect the current results. Therefore, we created a smaller VTA/SNc mask (size = 96 mm^3) by stripping off a layer of one voxel and reran the analysis. The smaller VTA/SNc seed showed almost identical one-sample *t*-test results across 250 subjects

Table 3 Regions showing greater connectivity with VTA/SNc when compared with the LC; paired *t*-test, $n = 250$

Volume (mm^3)	Peak voxel (Z)	MNI coordinate			Side	Identified brain region	Connectivity	
		x	y	z			LC	VTA/SNc
185 544	Inf	6	−16	−14	R	Midbrain/insula/vpallidum/vputamen/PHG/ITC/MCC/PCC	+	++
	Inf	−6	−16	−14	L	Midbrain/insula/vpallidum/vputamen/PHG/ITC/MCC/PCC	+	++
	Inf	9	−16	7	R	Thalamus*	~	+
17 037	Inf	0	−94	−14	R/L	Calcarine sulcus	− −	−
	Inf	−9	−91	−26	L	Cerebellum (posterior and lateral cortex)	−	~
25 164	7.76	3	62	−5	R	mOFC/vmPFC/dmPFC	−/~/~	~/+/+

Inf: infinity; R: right; L: left; vpallidum: ventral pallidum; vputamen: ventral putamen; PHG: parahippocampal gyrus; ITC: inferior temporal cortex; MCC: middle cingulate cortex; PCC: posterior cingulate cortex; vmPFC: ventromedial prefrontal cortex; dmPFC: dorsomedial prefrontal cortex; *: with subareal variation; +/−: positive and negative connectivity (with ++/− − for stronger connectivity); ~: non-significant connectivity at one-sample *t*-test, $P < 0.05$, FWE-corrected.

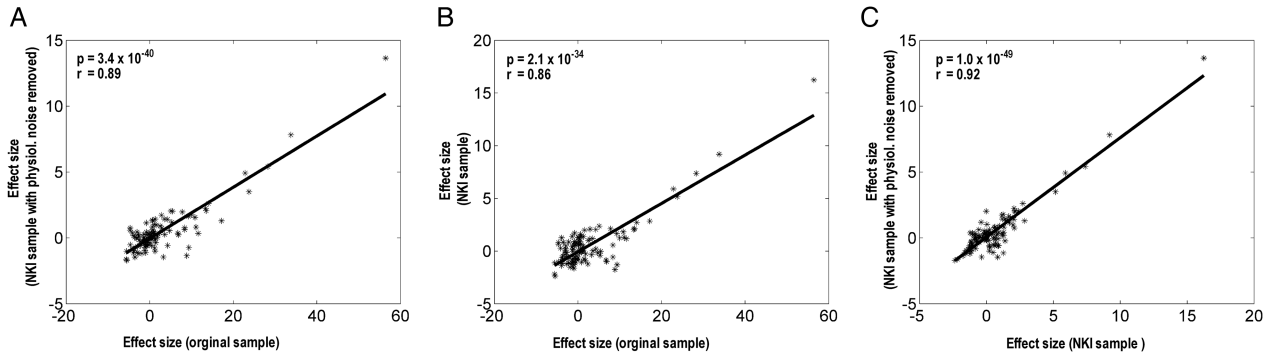

Figure 3. Pairwise regressions of the effect size of LC connectivity to the 116 AAL regions between the original sample, NKI sample, and NKI with physiological noise removed.

when compared with the original seed. A comparison of connectivity between the smaller VTA/SNc and LC also yielded very similar results as in the contrast between the original VTA/SNc and LC seeds (Supplementary Fig. 3).

We further examined the reliability and reproducibility of the results by rerunning the analysis using an open access test–retest dataset: NYU CSC TestRetest, which is fully available via http://www.nitrc.org/projects/nyu_trt (Zuo, Di Martino, et al. 2010; Zuo, Kelly, et al. 2010). The results suggested that the main findings were the same (Supplementary Figs 4 and 5).

Shared Cerebral Connectivity Between the LC and VTA/SNc

The LC and VTA/SNc shared positive connectivity (PosR) to putamen, pallidum, posterior insula, ventrolateral thalamus, midbrain, and large areas of the cerebellum (Fig. 4A, red). The LC and VTA/SNc shared negative connectivity (NegR) to the bilateral visual cortex, temporal cortex, precuneus, caudate nucleus, and dorsomedial thalamus (Fig. 4A, blue). These shared connectivities may reflect the common metabolic pathways and signaling mechanisms norepinephrine and dopamine partake in, as discussed in the Introduction section. In addition, bilateral amygdala, right anterior insula/inferior frontal cortex, pars orbitalis, and pulvinar showed negative connectivity to LC and positive connectivity to VTA/SNc (Fig. 4A, green). No brain regions showed both significant positive connectivity to LC and negative connectivity to VTA/SNc.

We further examined whether LC and VTA/SNc connectivities to the "shared" regions are correlated across subjects. As described in the Materials and Methods section, because some of the areas with shared connectivity comprised multiple regions, we used anatomical masks to further distinguish the regions within each cluster. As a result, we have 11 regions with PosR, 9 regions with NegR, and 3 regions with negative connectivity to LC and positive connectivity to VTA/SNc (LC_NegR and VTA_PosR). These individual regions are labeled in Figure 4. For each of these regions, we performed a linear regression of LC and VTA/SNc connectivities across subjects. Figure 4 showed a matrix of the *r* values for regressions that were significant at $P < 0.05$ corrected for 211 ($11^2 + 9^2 + 3^2$) comparisons (i.e., uncorrected $P < 0.05/211 = 0.000237$). All of these regions showed a significant correlation in LC and VTA/SNc connectivity, irrespective of its sign, across subjects. Of all positive connectivities to both seeds, about one-third (33.9%) showed a significant positive cross-regional correlation (Fig. 4B). Of all negative connectivities to both seeds, 14.8% showed a cross-regional correlation (Fig. 4C).

The Effects of Age and Gender on LC and VTA/SNc Connectivity

In a simple regression, LC connectivity to the angular gyrus, middle frontal gyrus, as well as cerebellum showed positive correlations with age and LC connectivity to the parahippocampus, parietal–occipital fissure, precuneus, and cuneus showed negative correlations with age (Fig. 5A and Table 4). VTA/SNc connectivity to the superior and middle frontal gyri and cerebellum showed positive correlation and to the postcentral gyrus showed a negative correlation with age (Fig. 5B and Table 4).

In a covariance analysis with age as a covariate, we examined gender differences. Men showed greater connectivity between LC and midbrain, hippocampus, parahippocampus, and middle temporal gyrus than women (Fig. 5C and Table 5). There is no gender difference for VTA/SNc connectivity.

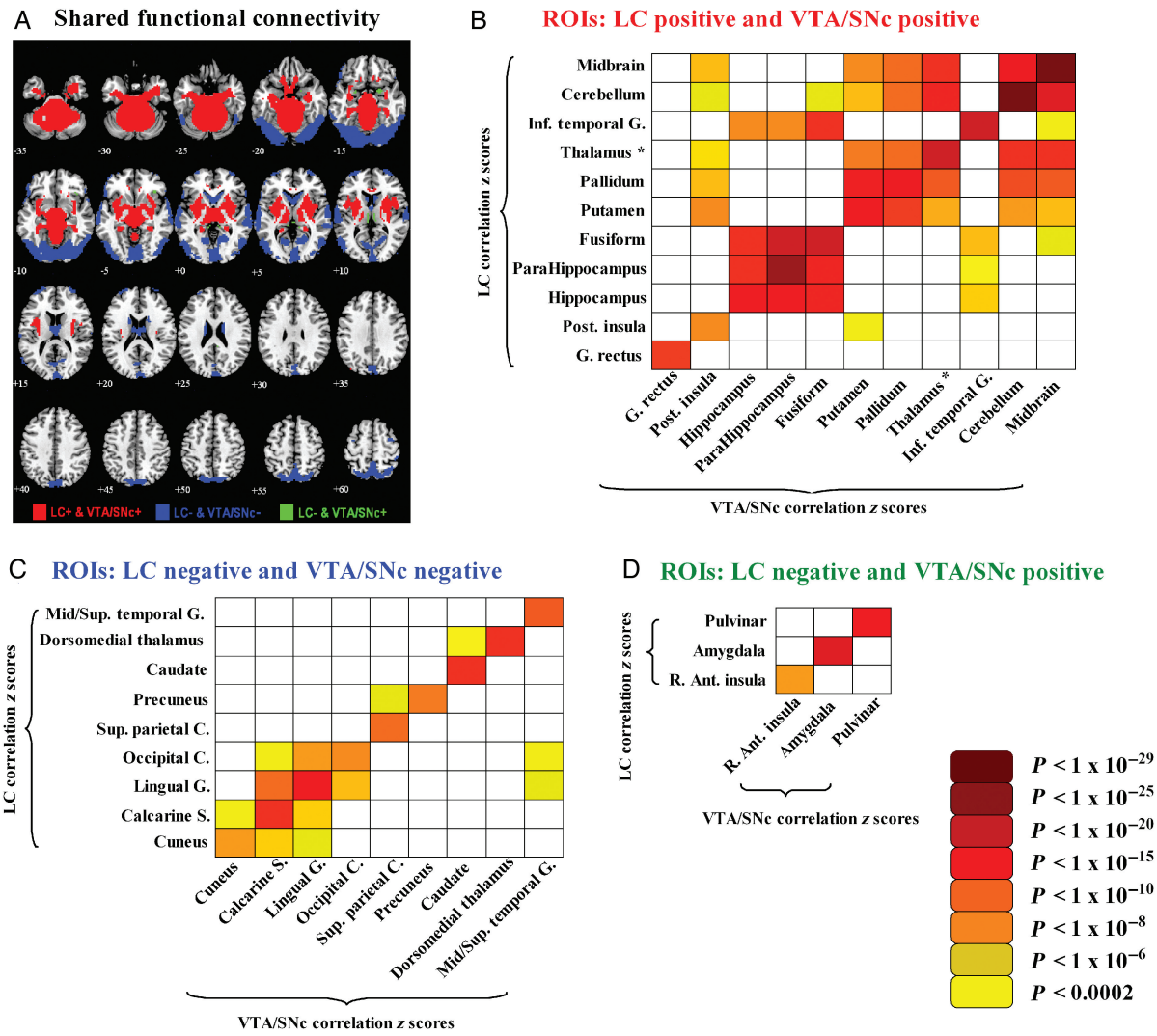

Figure 4. (*A*) Brain areas that shared functional connectivity to the LC and VTA/SNc—positive connectivity (red color); negative connectivity (blue color); and negative connectivity to LC and positive connectivity to VTA/SNc (green color). (*B–D*) Matrices of *R* values of linear regressions ($P < 0.05$ corrected for multiple comparisons) between effect size (*z* scores) of ROIs with shared LC and VTA/SNc connectivity across all 250 subjects. There were 11 ROIs with PosR (red), 9 ROIs with NegR (blue), and 3 ROIs with negative connectivity to LC but positive connectivity to VTA/SNc (green). Asterisk: except dorsomedial thalamus; Inf.: inferior; G.: gyrus; Post.: posterior; R.: right; Ant.: anterior; Mid.: middle; Sup.: superior; C.: cortex; S.: sulcus.

Discussion

Functional Connectivity Shared Between the LC and VTA/SNc

The LC showed both shared and distinct cerebral connectivity, when compared with VTA/SNc. The LC and VTA/SNc PosR to putamen, pallidum, posterior insula, ventrolateral thalamus, midbrain, and large areas of the cerebellum; and NegR to bilateral visual cortex, middle/superior temporal cortex, precuneus, posterior cingulate cortex, caudate nucleus, and medial thalamus. The posterior insula receives inputs from primary sensory cortices (Craig 2011), and the putamen, pallidum, and ventrolateral thalamus comprise the striato-thalamic circuit that gates motor output (Hikosaka 2007; Li et al. 2008; Polania et al. 2012). In support of our hypothesis of shared NA and DA connectivity, these results suggest a role of both the NA and DA systems in orienting and sensorimotor responses to external stimuli. Furthermore, LC and VTA/SNc each has widespread connectivities, and thus, the current findings do not appear to mirror studies of histochemistry that reported a more general NA and restricted DA cerebral distributions (Levitt et al. 1984).

A few issues are notable from these findings. First, although a vast literature supports DA innervations of the striatum, the current results provide evidence for NA modulation of the striatal circuits, whether the modulation is mediated by direct or collateral anatomical projections (Room et al. 1981; Moore and Card 1984); LC and VTA/SNc connectivities to the putamen and pallidum are highly correlated across subjects ($P < 1 \times 10^{-12}$; Fig. 4). Similarly, while the thalamus has largely been thought of receiving only NA inputs from the midbrain (Jones 2007), the current findings demonstrate DA modulation of thalamic activity, and the strength of NA and DA connectivities are correlated across subjects for ventrolateral ($P < 1 \times 10^{-21}$; LC and VTA/SNc connectivity both positive) and dorsomedial ($P < 1 \times 10^{-13}$; LC and VTA/SNc connectivity both negative) thalamus. This finding is consistent with more recent work showing concentration of dopamine transporter in the mediodorsal and ventral motor thalamus in macaque monkeys (Garcia-Cabezas et al. 2009).

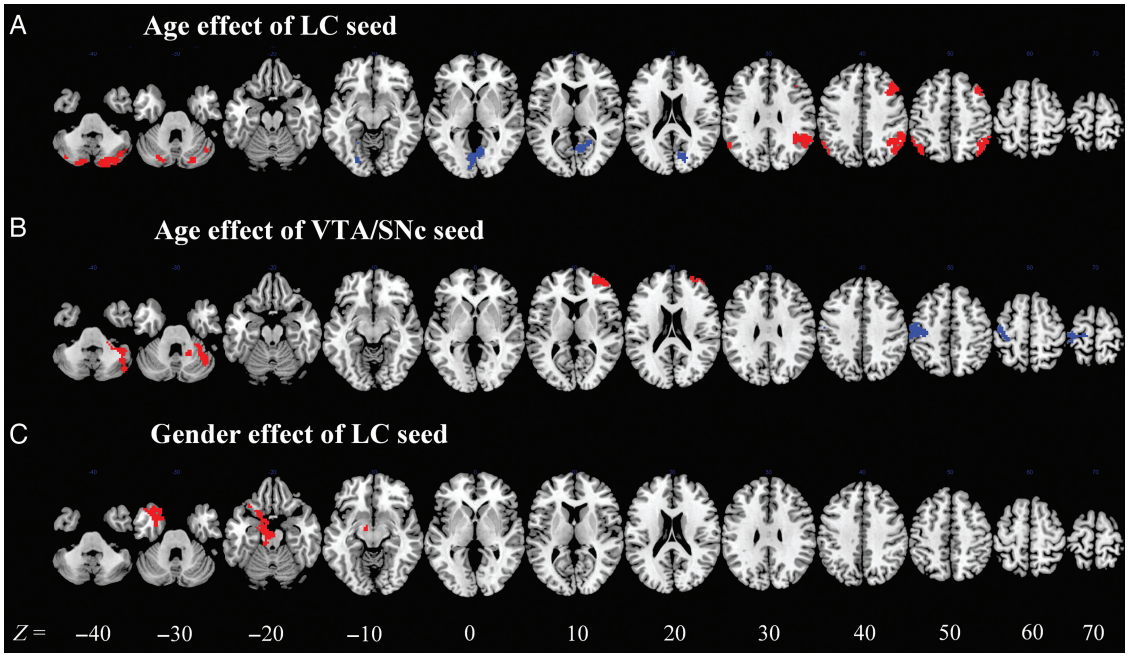

Figure 5. Brain areas where functional connectivity to the (*A*) LC and (*B*) VTA/SNc correlates positively (red) and negatively (blue) with age. (*C*) Brain regions showing gender differences in LC connectivity (red: male > female). VTA/SNc connectivity did not show any gender differences. Voxel-level $P < 0.001$ uncorrected and cluster-level $P < 0.05$, FWE-corrected.

Table 4 Age correlation in seed-based connectivity

Volume (mm^3)	Peak voxel (Z)	MNI coordinate			Side	Identified brain region
		x	y	z		
Positive correlation, LC						
10 935	5.13	54	−49	37	R	Angular gyrus/inferior parietal cortex
8370	4.59	21	−82	−50	R	Cerebellum
2997	4.33	−15	−85	−41	L	Cerebellum
3105	4.14	−42	−67	52	L	Angular gyrus/inferior parietal cortex
3159	4.06	42	20	43	R	Middle frontal gyrus
Negative correlation, LC						
10 044	4.27	6	−61	7	R	Lingual gyrus/calcarine sulcus
Positive correlation, VTA/SNc						
7776	4.67	39	−46	−50	R	Cerebellum
3051	4.22	30	56	13	R	Superior/middle frontal gyrus
Negative correlation, VTA/SNc						
7746	4.29	−51	−16	49	L	Postcentral gyrus

Note: voxel $P < 0.001$ uncorrected and cluster-level $P < 0.05$, FWE-corrected.
R: right; L: left.

Second, both LC and VTA/SNc showed positive connectivity to the putamen and pallidum but negative connectivity to the caudate head. This suggests that the caudate head is functionally distinct from the sensorimotor striatum (Arsalidou et al. 2013), consistent with differential dorsomedial prefrontal connectivities of these striatal subregions (Zhang et al. 2012). While sensorimotor striatum is connected to the primary motor areas and SMA, the caudate is connected to the pre-SMA (Di Martino et al. 2008; Zhang et al. 2012). Thus, LC and VTA/SNc connectivity entrain the putamen and pallidum in rapid actions to external stimuli, but these ascending inputs may suppress immediate caudate response in favor of planned actions (Grahn et al. 2008). Third, consistent with known functions of the default network, LC and VTA/SNc negatively modulate the precuneus. That is, the default network regions deactivate in responses to environmental stimuli, as part of an "alert and orient" system (Li et al. 2007; Zhang and Li 2010, 2012a, 2012c).

Differences in Functional Connectivity of the LC and VTA/SNc

LC and VTA/SNc also showed differences in functional connectivities. Compared with the VTA/SNc, LC showed less negative connectivity to bilateral visual, parietal, and somatomotor cortices, as well as greater positive connectivity to midline cerebellar structures. In addition, LC showed less positive connectivity to ventromedial and dorsomedial prefrontal cortex, middle and posterior cingulate cortex, inferior temporal cortex, ventral

Table 5 Gender differences in seed-based connectivity

Volume (mm^3)	Peak voxel (Z)	MNI coordinate			Side	Identified brain region
		x	y	z		
Men > women, LC						
9099	4.90	−9	−28	−23	L	Midbrain/hippocampus/parahippocampus
	4.68	−30	11	−32	L	Middle temporal gyrus
Women > men, LC						
None						
Men > women, VTA/SNc						
None						
Women > men, VTA/SNc						
None						

Note: voxel $P < 0.001$ uncorrected and cluster-level $P < 0.05$, FWE-corrected.
R: right; L: left.

pallidum and putamen, anterior insula, thalamus, and the midbrain. The latter findings are consistent with more extensive DA innervation of the ventral striatum, parahippocampal gyrus, and midline brain regions, as we posited. However, more broadly, it is difficult to relate these findings to the extent of NA and DA innervations of the various cortical and subcortical structures, as studies of neurochemical mapping did not directly contrast the 2 systems (Simpson et al. 1997; Sanchez-Gonzalez et al. 2005). A few findings from the literature seem consistent with these findings. For instance, DA agonists are known to suppress visually evoked myoclonus or epileptic seizures (Quesney et al. 1980; Obeso et al. 1985) in accord with negative VTA/SNc connectivity to sensorimotor cortex. Greater positive VTA/SNc than LC connectivity to the dorsomedial prefrontal cortex is consistent with DA signal in mediating prediction error (Schultz and Dickinson 2000; Aggarwal et al. 2012; Ide et al. 2013). It is also possible that, while the LC supports a general state or arousal, the VTA/SNc is involved in titrating moment-to-moment need to support goal-directed behavior. The finding of less LC than VTA/SNc connectivity to the thalamus seems at odds with previous reports of heavy concentration of NET in the thalamus (Ding et al. 2003). On the other hand, with manganese-enhanced MRI, Eschenko et al. (2012) identified only sparse LC projections to the thalamus. One possibility is that extracellular dopamine in the cerebral cortex and thalamus may originate not only from DA but also from NA terminals (Devoto and Flore 2006, for a review), and the NET serves to regulate synaptic turnover of not only norepinephrine but also dopamine in the thalamus (Moron et al. 2002). There is a notable difference in subregional connectivity in the thalamus. While ventrolateral/posterior thalamus showed positive connectivity to both the LC and VTA/SNc, less positivity connectivity is observed, with the dorsal and medial thalamus showing greater negative connectivity, to the LC. These observations speak to the importance in clearly delineating subregions in characterizing thalamic activations and connectivities.

Opposing Pattern of Connectivity Between the LC and VTA/SNc

Bilateral amygdala, right anterior insula (bordering the inferior frontal cortex pars orbitalis), and pulvinar showed negative connectivity to LC and positive connectivity to VTA/SNc. Amygdala, insula, and the pulvinar are part of a neural circuit that responds to salient stimuli (Hayes and Northoff 2012). Neurons in both LC and VTA/SNc exhibit phasic discharges to salient environmental stimuli and facilitate activities of their target neurons (Aston-Jones and Cohen 2005; Grace et al. 2007). However, LC and VTA/SNc neurons also maintain a tonic discharge, and the interacting influences of the tonic and phasic activities on target neurons are complex and dependent on behavioral states and contingencies (Aston-Jones and Cohen 2005; Devilbiss and Waterhouse 2011). Nonetheless, in an earlier study, electrical stimulation of the LC decreased responses of thalamic neurons to visual stimulation (Holdefer and Jacobs 1994). In another study, norepinephrine iontophoresis inhibited spontaneous firing and decreased the responsiveness of amygdala neurons to electrical stimulation of input regions (Buffalari and Grace 2007). Amygdala receives heavy projections from the VTA. While studies support DA regulation of amygdala activities during fear conditioning, there is a paucity of literature examining the interaction between VTA and amygdala neurons (Walsh and Han 2014). Likewise, there are, to our knowledge, no studies examining the interaction between the 2 midbrain nuclei and the insula or pulvinar. To fully explain the opposing patterns of functional connectivity of LC and VTA/SNc to these 3 structures would require more studies and considerations that go beyond direct catecholaminergic projections.

Comparison with Anatomical Mapping of LC and VTA/SNc in Animals

We summarized and contrasted the connectivity findings with previous anatomical studies in monkeys, cats, and rodents (Supplementary Table 1). The results appeared largely consistent, with very few brain regions showing functional connectivity (either positive or negative) in humans but not anatomical connectivity in animals or vice versa. On the other hand, one is to caution against over-interpretation of these comparisons as identically named entities may represent functionally distinct structures across species.

Age-Related Connectivity of the LC

Previous imaging studies suggest that aging is related in a complicated way to cerebral functional connectivities, with different brain areas increasing and decreasing with age in connectivity to ROIs [Taniwaki et al. 2007; Ystad et al. 2010; Liu et al. 2012; Bernard et al. 2013; Campbell et al. 2013; Hafkemeijer et al. 2013; Roski et al. 2013; Hoffstaedter et al. 2015; see also Ferreira and Busatto (2013) for a review]. Here, we observed that age is associated with increased LC connectivity to angular gyrus, middle frontal gyrus, as well as cerebellum and decreased LC

connectivity to the parahippocampus, parietal–occipital fissure, precuneus, and cuneus. The latter finding is consistent with a recent report of decreased LC parahippocampal connectivity in association with working memory deficits in elderly individuals with mild cognitive impairment (Jacobs et al. 2015). Along with work of age-related changes in the functional connectivity of the VTA (Tomasi and Volkow 2014), these findings may further our understanding of the pathophysiology of Alzheimer's disease, Parkinson's disease, and other degenerative conditions that implicate the catecholaminergic systems [Delaville et al. 2011; Isaias et al. 2011; Del Tredici and Braak 2013; Liu et al. 2013; Mravec et al. 2014; Takahashi et al. 2015; Jacobs et al. 2015; see also Trillo et al. (2013) for a review].

A Methodological Consideration

Negative functional connectivity has been observed and reported since the very beginning of the resting-state fMRI study (Biswal et al. 1995). Negative functional connectivity, also called anti-correlation, represents negative cross-correlation in spontaneous BOLD signal between 2 brain regions. It was suggested that the global signal regression, a common step of data preprocessing in seed region-based functional connectivity analyses, is a likely cause of anti-correlated functional networks (Murphy et al. 2009; Weissenbacher et al. 2009). However, other investigations demonstrated that the negative correlations are not an artifact, but have biological origins (Fox et al. 2009; Chen et al. 2011; Chai et al. 2012). For instance, negative functional connectivity is associated predominantly with long-range connections and correlates with the shortest path length in the human brain network (Scholvinck et al. 2010; Chen et al. 2011; Schwarz and McGonigle 2011). Indeed, the negative correlations between brain regions with presumably opposing functional roles have been consistently observed in different studies (Greicius et al. 2003; Fox et al. 2005; Fransson 2005; Kelly et al. 2008; Uddin et al. 2009; Chen et al. 2011), including those using independent component analysis, which does not involve global signal regression (Cole et al. 2010; Zuo, Kelly, et al. 2010; Zhang and Li 2012b). Furthermore, the existence of the negative functional connectivity was also suggested by computational simulations of cerebral network activities in both monkeys and humans (Honey et al. 2007; Izhikevich and Edelman 2008; Deco et al. 2009) and supported by simultaneous recording of unit activity and local field potential from task-positive and task-negative (default mode) networks in cats (Popa et al. 2009). Taken together, these earlier studies suggest functional significance of negative functional connectivity.

Limitations of the Study and Conclusions

There are a few limitations to consider. First, small size of the LC has hampered imaging research of the NA systems in humans. Here, we took advantage of a probabilistic template to identify resting-state functional connectivities of the LC. We used both a smoothing kernel of 8 and 4 mm in order to examine LC connectivity to both cortical and subcortical structures (Hopfinger et al. 2000) and observed very similar results. Furthermore, we identified a data set with concurrent recording of cardiac and respiratory signals. While the small sample size may pose issues to a direct comparison of results, ROI analyses suggested that the patterns of functional connectivity as reported for the original sample are independent of the physiological confounds. Moreover, because of the small size of the LC, intersubject variation in registration to a common template may affect the results. A recent study examined resting-state functional connectivity of the LC in both healthy individuals and early dementia patients (Jacobs et al. 2015). Registering the LC to each individual's T_1-weighted image by a high-resolution binary template previously validated in vivo, the authors reported positive connectivities to the hippocampus/parahippocampus as with the current findings. Nonetheless, small seed volume and low-resolution images remain critical issues, and the results need to be confirmed by higher resolution imaging. Second, it is important to note that functional connectivities between the LC and cerebral cortex are task-dependent (Coull et al. 1999), and that resting-state connectivities do not distinguish between tonic and phasic neuronal activities that are of distinct importance to cerebral functioning (Minzenberg et al. 2008). For instance, enhancing NA signaling with reboxetine increased activity in the right visual and fronto-parietal cortex during goal-directed hand movements (Grefkes et al. 2010), seemingly in contrast to the current finding of a negative connectivity between the LC and visual and parietal cortices. Without measures of behavioral performance, one cannot extrapolate functional relevance from the current findings. Third, it is important to note that the current sample contains participants in young to middle adulthood. Thus, the age-related findings should be considered as specific to this age range. Future research is needed to understand changes in LC connectivity in the elderly. Fourth, we did not distinguish between VTA and SNc which may show different patterns of connectivity that warrants further investigation (Kwon and Jang 2014). Likewise, LC neurons innervating discrete cortical regions are biochemically and electrophysiologically distinct, suggesting the complexity in characterizing LC connectivity as a whole (Chandler, Gao, et al. 2014). Finally, because extant work investigated NA or DA innervations separately (Lewis and Morrison 1989), immunohistochemical studies to examine the distribution of "both" systems in the same animals are needed to confirm the anatomical validity of these findings.

To conclude, LC showed a distinct pattern of cerebral functional connectivity that enhances attentional orienting and sensorimotor responses to salient stimuli. Taken together with recent work characterizing VTA/SNc connectivity, the current findings may have important implications for future research to characterize the distinct roles of NA and DA modulation of cerebral activations and connectivities during rest or task challenges in health and illness (Mueller et al. 2014).

Supplementary material

Supplementary Material can be found at: http://www.cercor.oxfordjournals.org/.

Funding

This study was supported by the NIH grants DA023248, DA026990, AA018004, and AA021449. The NIH had no further role in study design; in the collection, analysis, and interpretation of data; in the writing of the report; or in the decision to submit the paper for publication.

Notes

We are grateful to Drs Noam Keren and Mark Eckert of the Medical University of South Carolina for sharing the LC mask. We also thank investigators of the 1000 Functional Connectomes Project and those who shared the data set for making this study possible.
Conflict of Interest: None declared.

References

Agarwal RK, Chandna VK, Engelking LR, Lightbown K, Kumar MS. 1993. Distribution of catecholamines in the central nervous system of the pig. Brain Res Bull. 32:285–291.

Aggarwal M, Hyland BI, Wickens JR. 2012. Neural control of dopamine neurotransmission: implications for reinforcement learning. Eur J Neurosci. 35:1115–1123.

Ahsan RL, Allom R, Gousias IS, Habib H, Turkheimer FE, Free S, Lemieux L, Myers R, Duncan JS, Brooks DJ, et al. 2007. Volumes, spatial extents and a probabilistic atlas of the human basal ganglia and thalamus. Neuroimage. 38:261–270.

al-Tikriti MS, Zea-Ponce Y, Baldwin RM, Zoghbi SS, Laruelle M, Seibyl JP, Giddings SS, Scanley BE, Charney DS, Hoffer PB, et al. 1995. Characterization of the dopamine transporter in nonhuman primate brain: homogenate binding, whole body imaging, and ex vivo autoradiography using [^{125}I] and [^{123}I] IPCIT. Nucl Med Biol. 22:649–658.

Arnsten AF. 2007. Catecholamine and second messenger influences on prefrontal cortical networks of "representational knowledge": a rational bridge between genetics and the symptoms of mental illness. Cereb Cortex. 17(Suppl 1):i6–15.

Arnsten AF, Li BM. 2005. Neurobiology of executive functions: catecholamine influences on prefrontal cortical functions. Biol Psychiatry. 57:1377–1384.

Arsalidou M, Duerden EG, Taylor MJ. 2013. The centre of the brain: topographical model of motor, cognitive, affective, and somatosensory functions of the basal ganglia. Hum Brain Mapp. 34:3031–3054.

Ashburner J, Friston KJ. 1999. Nonlinear spatial normalization using basis functions. Hum Brain Mapp. 7:254–266.

Aston-Jones G, Cohen JD. 2005. Adaptive gain and the role of the locus coeruleus-norepinephrine system in optimal performance. J Comp Neurol. 493:99–110.

Baldo BA, Daniel RA, Berridge CW, Kelley AE. 2003. Overlapping distributions of orexin/hypocretin- and dopamine-beta-hydroxylase immunoreactive fibers in rat brain regions mediating arousal, motivation, and stress. J Comp Neurol. 464:220–237.

Bari A, Robbins TW. 2013. Inhibition and impulsivity: behavioral and neural basis of response control. Prog Neurobiol. 108:44–79.

Barnes KA, Cohen AL, Power JD, Nelson SM, Dosenbach YB, Miezin FM, Petersen SE, Schlaggar BL. 2010. Identifying basal ganglia divisions in individuals using resting-state functional connectivity MRI. Front Syst Neurosci. 4:18.

Bernard JA, Peltier SJ, Wiggins JL, Jaeggi SM, Buschkuehl M, Fling BW, Kwak Y, Jonides J, Monk CS, Seidler RD. 2013. Disrupted cortico-cerebellar connectivity in older adults. Neuroimage. 83:103–119.

Berry KJ, Mielke PW Jr. 2000. A Monte Carlo investigation of the Fisher Z transformation for normal and nonnormal distributions. Psychol Rep. 87:1101–1114.

Biswal B, Yetkin FZ, Haughton VM, Hyde JS. 1995. Functional connectivity in the motor cortex of resting human brain using echo-planar MRI. Magn Reson Med. 34:537–541.

Biswal BB, Mennes M, Zuo XN, Gohel S, Kelly C, Smith SM, Beckmann CF, Adelstein JS, Buckner RL, Colcombe S, et al. 2010. Toward discovery science of human brain function. Proc Natl Acad Sci USA. 107:4734–4739.

Buffalari DM, Grace AA. 2007. Noradrenergic modulation of basolateral amygdala neuronal activity: opposing influences of alpha-2 and beta receptor activation. J Neurosci. 27: 12358–12366.

Bymaster FP, Katner JS, Nelson DL, Hemrick-Luecke SK, Threlkeld PG, Heiligenstein JH, Morin SM, Gehlert DR, Perry KW. 2002. Atomoxetine increases extracellular levels of norepinephrine and dopamine in prefrontal cortex of rat: a potential mechanism for efficacy in attention deficit/hyperactivity disorder. Neuropsychopharmacology. 27:699–711.

Campbell KL, Grigg O, Saverino C, Churchill N, Grady CL. 2013. Age differences in the intrinsic functional connectivity of default network subsystems. Front Aging Neurosci. 5:73.

Carboni E, Silvagni A, Vacca C, Di Chiara G. 2006. Cumulative effect of norepinephrine and dopamine carrier blockade on extracellular dopamine increase in the nucleus accumbens shell, bed nucleus of stria terminalis and prefrontal cortex. J Neurochem. 96:473–481.

Cauda F, Geminiani G, D'Agata F, Sacco K, Duca S, Bagshaw AP, Cavanna AE. 2010. Functional connectivity of the posteromedial cortex. PLoS ONE. 5(9):e13107. doi:10.1371/journal.pone.0013107

Caveney S, Cladman W, Verellen L, Donly C. 2006. Ancestry of neuronal monoamine transporters in the Metazoa. J Exp Biol. 209:4858–4868.

Chai XJ, Castanon AN, Ongur D, Whitfield-Gabrieli S. 2012. Anticorrelations in resting state networks without global signal regression. Neuroimage. 59:1420–1428.

Chandler DJ, Gao WJ, Waterhouse BD. 2014. Heterogeneous organization of the locus coeruleus projections to prefrontal and motor cortices. Proc Natl Acad Sci USA. 111:6816–6821.

Chandler DJ, Lamperski CS, Waterhouse BD. 2013. Identification and distribution of projections from monoaminergic and cholinergic nuclei to functionally differentiated subregions of prefrontal cortex. Brain Res. 1522:38–58.

Chandler DJ, Waterhouse BD, Gao WJ. 2014. New perspectives on catecholaminergic regulation of executive circuits: evidence for independent modulation of prefrontal functions by midbrain dopaminergic and noradrenergic neurons. Front Neural Circuits. 8:53.

Chen G, Chen G, Xie C, Li SJ. 2011. Negative functional connectivity and its dependence on the shortest path length of positive network in the resting-state human brain. Brain Connectivity. 1:195–206.

Clark KL, Noudoost B. 2014. The role of prefrontal catecholamines in attention and working memory. Front Neural Circuits. 8:33.

Clewett D, Schoeke A, Mather M. 2014. Locus coeruleus neuromodulation of memories encoded during negative or unexpected action outcomes. Neurobiol Learn Mem. 111:65–70.

Colavito V, Tesoriero C, Wirtu AT, Grassi-Zucconi G, Bentivoglio M. 2015. Limbic thalamus and state-dependent behavior: the paraventricular nucleus of the thalamic midline as a node in circadian timing and sleep/wake-regulatory networks. Neurosci Biobehav Rev. 54:3–17.

Cole DM, Beckmann CF, Long CJ, Matthews PM, Durcan MJ, Beaver JD. 2010. Nicotine replacement in abstinent smokers improves cognitive withdrawal symptoms with modulation of resting brain network dynamics. Neuroimage. 52:590–599.

Cordes D, Haughton VM, Arfanakis K, Carew JD, Turski PA, Moritz CH, Quigley MA, Meyerand ME. 2001. Frequencies contributing to functional connectivity in the cerebral cortex in "resting-state" data. AJNR Am J Neuroradiol. 22:1326–1333.

Cornil CA, Ball GF. 2008. Interplay among catecholamine systems: dopamine binds to alpha2-adrenergic receptors in birds and mammals. J Comp Neurol. 511:610–627.

Coull JT, Buchel C, Friston KJ, Frith CD. 1999. Noradrenergically mediated plasticity in a human attentional neuronal network. Neuroimage. 10:705–715.

Craig AD. 2011. Significance of the insula for the evolution of human awareness of feelings from the body. Ann N Y Acad Sci. 1225:72–82.

Deco G, Jirsa V, McIntosh AR, Sporns O, Kotter R. 2009. Key role of coupling, delay, and noise in resting brain fluctuations. Proc Natl Acad Sci USA. 106:10302–10307.

Delaville C, Deurwaerdere PD, Benazzouz A. 2011. Noradrenaline and Parkinson's disease. Front Syst Neurosci. 5:31.

Del Campo N, Chamberlain SR, Sahakian BJ, Robbins TW. 2011. The roles of dopamine and noradrenaline in the pathophysiology and treatment of attention-deficit/hyperactivity disorder. Biol Psychiatry. 69:e145–e157.

Del Tredici K, Braak H. 2013. Dysfunction of the locus coeruleus-norepinephrine system and related circuitry in Parkinson's disease-related dementia. J Neurol Neurosurg Psychiatry. 84:774–783.

Devilbiss DM, Waterhouse BD. 2011. Phasic and tonic patterns of locus coeruleus output differentially modulate sensory network function in the awake rat. J Neurophysiol. 105:69–87.

Devoto P, Flore G. 2006. On the origin of cortical dopamine: is it a co-transmitter in noradrenergic neurons? Curr Neuropharmacol. 4:115–125.

Di Martino A, Scheres A, Margulies DS, Kelly AM, Uddin LQ, Shehzad Z, Biswal B, Walters JR, Castellanos FX, Milham MP. 2008. Functional connectivity of human striatum: a resting state FMRI study. Cereb Cortex. 18:2735–2747.

Ding YS, Lin KS, Garza V, Carter P, Alexoff D, Logan J, Shea C, Xu Y, King P. 2003. Evaluation of a new norepinephrine transporter PET ligand in baboons, both in brain and peripheral organs. Synapse. 50:345–352.

Dreher JC, Meyer-Lindenberg A, Kohn P, Berman KF. 2008. Age-related changes in midbrain dopaminergic regulation of the human reward system. Proc Natl Acad Sci USA. 105:15106–15111.

Eschenko O, Evrard HC, Neves RM, Beyerlein M, Murayama Y, Logothetis NK. 2012. Tracing of noradrenergic projections using manganese-enhanced MRI. Neuroimage. 59:3252–3265.

Fahn S, Libsch LR, Cutler RW. 1971. Monoamines in the human neostriatum: topographic distribution in normals and in Parkinson's disease and their role in akinesia, rigidity, chorea, and tremor. J Neurol Sci. 14:427–455.

Fair DA, Schlaggar BL, Cohen AL, Miezin FM, Dosenbach NU, Wenger KK, Fox MD, Snyder AZ, Raichle ME, Petersen SE. 2007. A method for using blocked and event-related fMRI data to study "resting state" functional connectivity. Neuroimage. 35:396–405.

Ferreira LK, Busatto GF. 2013. Resting-state functional connectivity in normal brain aging. Neurosci Biobehav Rev. 37:384–400.

Fox MD, Raichle ME. 2007. Spontaneous fluctuations in brain activity observed with functional magnetic resonance imaging. Nat Rev Neurosci. 8:700–711.

Fox MD, Snyder AZ, Vincent JL, Corbetta M, Van Essen DC, Raichle ME. 2005. The human brain is intrinsically organized into dynamic, anticorrelated functional networks. Proc Natl Acad Sci USA. 102:9673–9678.

Fox MD, Zhang D, Snyder AZ, Raichle ME. 2009. The global signal and observed anticorrelated resting state brain networks. J Neurophysiol. 101:3270–3283.

Fransson P. 2005. Spontaneous low-frequency BOLD signal fluctuations: an fMRI investigation of the resting-state default mode of brain function hypothesis. Hum Brain Mapp. 26:15–29.

Friston K, Ashburner J, Frith C, Polone J, Heather J, Frackowiak R. 1995. Spatial registration and normalization of images. Hum Brain Mapp. 2:165–189.

Garcia-Cabezas MA, Martinez-Sanchez P, Sanchez-Gonzalez MA, Garzon M, Cavada C. 2009. Dopamine innervation in the thalamus: monkey versus rat. Cereb Cortex. 19:424–434.

German DC, Walker BS, Manaye K, Smith WK, Woodward DJ, North AJ. 1988. The human locus coeruleus: computer reconstruction of cellular distribution. J Neurosci. 8:1776–1788.

Ginsberg SD, Hof PR, Young WG, Morrison JH. 1993. Noradrenergic innervation of the hypothalamus of rhesus monkeys: distribution of dopamine-beta-hydroxylase immunoreactive fibers and quantitative analysis of varicosities in the paraventricular nucleus. J Comp Neurol. 327:597–611.

Goldman-Rakic PS, Brown RM. 1981. Regional changes of monoamines in cerebral cortex and subcortical structures of aging rhesus monkeys. Neuroscience. 6:177–187.

Grace AA, Floresco SB, Goto Y, Lodge DJ. 2007. Regulation of firing of dopaminergic neurons and control of goal-directed behaviors. Trends Neurosci. 30:220–227.

Grahn JA, Parkinson JA, Owen AM. 2008. The cognitive functions of the caudate nucleus. Prog Neurobiol. 86:141–155.

Grefkes C, Wang LE, Eickhoff SB, Fink GR. 2010. Noradrenergic modulation of cortical networks engaged in visuomotor processing. Cereb Cortex. 20:783–797.

Greicius MD, Krasnow B, Reiss AL, Menon V. 2003. Functional connectivity in the resting brain: a network analysis of the default mode hypothesis. Proc Natl Acad Sci USA. 100:253–258.

Gu H, Salmeron BJ, Ross TJ, Geng X, Zhan W, Stein EA, Yang Y. 2010. Mesocorticolimbic circuits are impaired in chronic cocaine users as demonstrated by resting-state functional connectivity. Neuroimage. 53:593–601.

Hadley JA, Nenert R, Kraguljac NV, Bolding MS, White DM, Skidmore FM, Visscher KM, Lahti AC. 2014. Ventral tegmental area/midbrain functional connectivity and response to antipsychotic medication in schizophrenia. Neuropsychopharmacology. 39:1020–1030.

Hafkemeijer A, Altmann-Schneider I, Oleksik AM, van de Wiel L, Middelkoop HA, van Buchem MA, van der Grond J, Rombouts SA. 2013. Increased functional connectivity and brain atrophy in elderly with subjective memory complaints. Brain Connectivity. 3:353–362.

Hamon M, Blier P. 2013. Monoamine neurocircuitry in depression and strategies for new treatments. Prog Neuropsychopharmacol Biol Psychiatry. 45:54–63.

Harley C. 1991. Noradrenergic and locus coeruleus modulation of the perforant path-evoked potential in rat dentate gyrus supports a role for the locus coeruleus in attentional and memorial processes. Prog Brain Res. 88:307–321.

Hayes DJ, Northoff G. 2012. Common brain activations for painful and non-painful aversive stimuli. BMC Neurosci. 13:60.

Herregodts P, Ebinger G, Michotte Y. 1991. Distribution of monoamines in human brain: evidence for neurochemical heterogeneity in subcortical as well as in cortical areas. Brain Res. 542:300–306.

Hikosaka O. 2007. GABAergic output of the basal ganglia. Prog. Brain Res. 160:209–226.

Hoffstaedter F, Grefkes C, Roski C, Caspers S, Zilles K, Eickhoff SB. 2015. Age-related decrease of functional connectivity additional to gray matter atrophy in a network for movement initiation. Brain Struct Funct. 222(2):999–1012.

Holdefer RN, Jacobs BL. 1994. Phasic stimulation of the locus coeruleus: effects on activity in the lateral geniculate nucleus. Exp. Brain Res. 100:444–452.

Honey CJ, Kotter R, Breakspear M, Sporns O. 2007. Network structure of cerebral cortex shapes functional connectivity on multiple time scales. Proc Natl Acad Sci USA. 104:10240–10245.

Hopfinger JB, Buchel C, Holmes AP, Friston KJ. 2000. A study of analysis parameters that influence the sensitivity of event-related fMRI analyses. Neuroimage. 11:326–333.

Hortnagl H, Schlogl E, Sperk G, Hornykiewicz O. 1983. The topographical distribution of the monoaminergic innervation in the basal ganglia of the human brain. Prog Brain Res. 58:269–274.

Huang RL, Wang CT, Tai MY, Tsai YF, Peng MT. 1995. Effects of age on dopamine release in the nucleus accumbens and amphetamine-induced locomotor activity in rats. Neurosci Lett. 200:61–64.

Ide JS, Shenoy P, Yu AJ, Li CS. 2013. Bayesian prediction and evaluation in the anterior cingulate cortex. J Neurosci. 33:2039–2047.

Isaias IU, Marzegan A, Pezzoli G, Marotta G, Canesi M, Biella GE, Volkmann J, Cavallari P. 2011. A role for locus coeruleus in Parkinson tremor. Front Hum Neurosci. 5:179.

Izhikevich EM, Edelman GM. 2008. Large-scale model of mammalian thalamocortical systems. Proc Natl Acad Sci USA. 105:3593–3598.

Jacobs HI, Wiese S, van de Ven V, Gronenschild EH, Verhey FR, Matthews PM. 2015. Relevance of parahippocampal-locus coeruleus connectivity to memory in early dementia. Neurobiol Aging. 36:618–626.

Jenkins GM, Watts DG. 1968. Spectral analysis and its applications. San Francisco: Holden-Day.

Jones EG. 2007. The thalamus. 2nd ed. New York (NY): Cambridge University Press.

Kahnt T, Chang LJ, Park SQ, Heinzle J, Haynes JD. 2012. Connectivity-based parcellation of the human orbitofrontal cortex. J Neurosci. 32:6240–6250.

Kahnt T, Tobler PN. 2013. Salience signals in the right temporoparietal junction facilitate value-based decisions. J Neurosci. 33:863–869.

Kelly AM, Uddin LQ, Biswal BB, Castellanos FX, Milham MP. 2008. Competition between functional brain networks mediates behavioral variability. Neuroimage. 39:527–537.

Keren NI, Lozar CT, Harris KC, Morgan PS, Eckert MA. 2009. In vivo mapping of the human locus coeruleus. Neuroimage. 47:1261–1267.

Kim JH, Lee JM, Jo HJ, Kim SH, Lee JH, Kim ST, Seo SW, Cox RW, Na DL, Kim SI, et al. 2010. Defining functional SMA and pre-SMA subregions in human MFC using resting state fMRI: functional connectivity-based parcellation method. Neuroimage. 49:2375–2386.

Kwon HG, Jang SH. 2014. Differences in neural connectivity between the substantia nigra and ventral tegmental area in the human brain. Front Hum Neuroscience. 8:41.

Levitt P, Rakic P, Goldman-Rakic P. 1984. Region-specific distribution of catecholamine afferents in primate cerebral cortex: a fluorescence histochemical analysis. J Comp Neurol. 227:23–36.

Lewis DA, Morrison JH. 1989. Noradrenergic innervation of monkey prefrontal cortex: a dopamine-beta-hydroxylase immunohistochemical study. J Comp Neurol. 282:317–330.

Li CS, Yan P, Bergquist KL, Sinha R. 2007. Greater activation of the "default" brain regions predicts stop signal errors. Neuroimage. 38:640–648.

Li CS, Yan P, Sinha R, Lee TW. 2008. Subcortical processes of motor response inhibition during a stop signal task. Neuroimage. 41:1352–1363.

Li SC. 2013. Neuromodulation and developmental contextual influences on neural and cognitive plasticity across the lifespan. Neurosci Biobehav Rev. 37:2201–2208.

Liu L, Luo S, Zeng L, Wang W, Yuan L, Jian X. 2013. Degenerative alterations in noradrenergic neurons of the locus coeruleus in Alzheimer's disease. Neural Regen Res. 8:2249–2255.

Liu Z, Bai L, Dai R, Zhong C, Wang H, You Y, Wei W, Tian J. 2012. Exploring the effective connectivity of resting state networks in mild cognitive impairment: an fMRI study combining ICA and multivariate Granger causality analysis. In: Conference Proceedings: Annual International Conference of the IEEE Engineering in Medicine and Biology Society IEEE Engineering in Medicine and Biology Society Annual Conference. pp. 5454–5457.

Lowe MJ, Mock BJ, Sorenson JA. 1998. Functional connectivity in single and multislice echoplanar imaging using resting-state fluctuations. Neuroimage. 7:119–132.

Macefield VG, James C, Henderson LA. 2013. Identification of sites of sympathetic outflow at rest and during emotional arousal: concurrent recordings of sympathetic nerve activity and fMRI of the brain. Int J Psychophysiol. 89:451–459.

Mackay AV, Yates CM, Wright A, Hamilton P, Davies P. 1978. Regional distribution of monoamines and their metabolites in the human brain. J Neurochem. 30:841–848.

Margulies DS, Kelly AM, Uddin LQ, Biswal BB, Castellanos FX, Milham MP. 2007. Mapping the functional connectivity of anterior cingulate cortex. Neuroimage. 37:579–588.

Margulies DS, Vincent JL, Kelly C, Lohmann G, Uddin LQ, Biswal BB, Villringer A, Castellanos FX, Milham MP, Petrides M. 2009. Precuneus shares intrinsic functional architecture in humans and monkeys. Proc Natl Acad Sci USA. 106:20069–20074.

Minzenberg MJ, Watrous AJ, Yoon JH, Ursu S, Carter CS. 2008. Modafinil shifts human locus coeruleus to low-tonic, high-phasic activity during functional MRI. Science. 322:1700–1702.

Moore RY, Card JP. 1984. Noradrenaline-containing neuron systems. In: Bjorklund A, Hokfelt T, editors. Handbook of Chemical Neuroanatomy. Amsterdam: Elsevier. p. 123–156.

Moret F, Guilland JC, Coudouel S, Rochette L, Vernier P. 2004. Distribution of tyrosine hydroxylase, dopamine, and serotonin in the central nervous system of amphioxus (*Branchiostoma lanceolatum*): implications for the evolution of catecholamine systems in vertebrates. J Comp Neurol. 468:135–150.

Moron JA, Brockington A, Wise RA, Rocha BA, Hope BT. 2002. Dopamine uptake through the norepinephrine transporter in brain regions with low levels of the dopamine transporter: evidence from knock-out mouse lines. J Neurosci. 22:389–395.

Moses SG, Robins E. 1975. Regional distribution of norepinephrine and dopamine in brains of depressive suicides and alcoholic suicides. Psychopharmacol Commun. 1:327–337.

Mravec B, Lejavova K, Cubinkova V. 2014. Locus (coeruleus) minoris resistentiae in pathogenesis of Alzheimer's disease. Curr Alzheimer Res. 11:992–1001.

Mueller S, Costa A, Keeser D, Pogarell O, Berman A, Coates U, Reiser MF, Riedel M, Moller HJ, Ettinger U, et al. 2014. The effects of methylphenidate on whole brain intrinsic functional connectivity. Hum Brain Mapp. 35(11):5379–5388.

Murphy K, Birn RM, Handwerker DA, Jones TB, Bandettini PA. 2009. The impact of global signal regression on resting state correlations: are anti-correlated networks introduced? Neuroimage. 44:893–905.

Murty VP, Shermohammed M, Smith DV, Carter RM, Huettel SA, Adcock RA. 2014. Resting state networks distinguish human ventral tegmental area from substantia nigra. Neuroimage. 100:580–589.

Nooner KB, Colcombe SJ, Tobe RH, Mennes M, Benedict MM, Moreno AL, Panek LJ, Brown S, Zavitz ST, Li Q, et al. 2012.

The NKI-Rockland Sample: a model for accelerating the pace of discovery science in psychiatry. Front Neurosci. 6:152.
Obeso JA, Artieda J, Tunon T, Luquin MR, Martinez Lage JM. 1985. Dopamine agonists suppress visual-cortical reflex myoclonus. J Neurol Neurosurg Psychiatry. 48:1277–1283.
O'Reilly JX, Beckmann CF, Tomassini V, Ramnani N, Johansen-Berg H. 2010. Distinct and overlapping functional zones in the cerebellum defined by resting state functional connectivity. Cereb Cortex. 20:953–965.
Panksepp J, Biven L. 2012. The archaeology of mind: the neuroevolutionary origins of human emotions. New York: Norton.
Park J, Wheeler RA, Fontillas K, Keithley RB, Carelli RM, Wightman RM. 2012. Catecholamines in the bed nucleus of the stria terminalis reciprocally respond to reward and aversion. Biol Psychiatry. 71:327–334.
Polania R, Paulus W, Nitsche MA. 2012. Modulating cortico-striatal and thalamo-cortical functional connectivity with transcranial direct current stimulation. Hum Brain Mapp. 33:2499–2508.
Popa D, Popescu AT, Pare D. 2009. Contrasting activity profile of two distributed cortical networks as a function of attentional demands. J Neurosci. 29:1191–1201.
Power JD, Barnes KA, Snyder AZ, Schlaggar BL, Petersen SE. 2012. Spurious but systematic correlations in functional connectivity MRI networks arise from subject motion. Neuroimage. 59:2142–2154.
Quesney LF, Andermann F, Lal S, Prelevic S. 1980. Transient abolition of generalized photosensitive epileptic discharge in humans by apomorphine, a dopamine-receptor agonist. Neurology. 30:1169–1174.
Rivera A, Penafiel A, Megias M, Agnati LF, Lopez-Tellez JF, Gago B, Gutierrez A, de la Calle A, Fuxe K. 2008. Cellular localization and distribution of dopamine D(4) receptors in the rat cerebral cortex and their relationship with the cortical dopaminergic and noradrenergic nerve terminal networks. Neuroscience. 155:997–1010.
Rombouts SA, Stam CJ, Kuijer JP, Scheltens P, Barkhof F. 2003. Identifying confounds to increase specificity during a "no task condition". Evidence for hippocampal connectivity using fMRI. Neuroimage. 20:1236–1245.
Room P, Postema F, Korf J. 1981. Divergent axon collaterals of rat locus coeruleus neurons: demonstration by a fluorescent double labeling technique. Brain Res. 221:219–230.
Roski C, Caspers S, Langner R, Laird AR, Fox PT, Zilles K, Amunts K, Eickhoff SB. 2013. Adult age-dependent differences in resting-state connectivity within and between visual-attention and sensorimotor networks. Front Aging Neurosci. 5:67.
Rubia K, Alegria AA, Cubillo AI, Smith AB, Brammer MJ, Radua J. 2014. Effects of stimulants on brain function in attention-deficit/hyperactivity disorder: a systematic review and meta-analysis. Biol Psychiatry. 76:616–628.
Sanchez-Gonzalez MA, Garcia-Cabezas MA, Rico B, Cavada C. 2005. The primate thalamus is a key target for brain dopamine. J Neurosci. 25:6076–6083.
Sarkka S, Solin A, Nummenmaa A, Vehtari A, Auranen T, Vanni S, Lin FH. 2012. Dynamic retrospective filtering of physiological noise in BOLD fMRI: DRIFTER. Neuroimage. 60:1517–1527.
Sasaki M, Shibata E, Tohyama K, Takahashi J, Otsuka K, Tsuchiya K, Takahashi S, Ehara S, Terayama Y, Sakai A. 2006. Neuromelanin magnetic resonance imaging of locus ceruleus and substantia nigra in Parkinson's disease. Neuroreport. 17:1215–1218.
Scholvinck ML, Maier A, Ye FQ, Duyn JH, Leopold DA. 2010. Neural basis of global resting-state fMRI activity. Proc Natl Acad Sci USA. 107:10238–10243.
Schonbachler RD, Gucker PM, Arigoni M, Kneifel S, Vollenweider FX, Buck A, Burger C, Berthold T, Bruhlmeier M, Schubiger PA, et al. 2002. PET imaging of dopamine transporters in the human brain using [(11)C]-beta-CPPIT, a cocaine derivative lacking the 2 beta-ester function. Nucl Med Biol. 29:19–27.
Schultz W, Dickinson A. 2000. Neuronal coding of prediction errors. Annu Rev Neurosci. 23:473–500.
Schwarz AJ, McGonigle J. 2011. Negative edges and soft thresholding in complex network analysis of resting state functional connectivity data. Neuroimage. 55:1132–1146.
Simpson KL, Altman DW, Wang L, Kirifides ML, Lin RC, Waterhouse BD. 1997. Lateralization and functional organization of the locus coeruleus projection to the trigeminal somatosensory pathway in rat. J Comp Neurol. 385:135–147.
Smith CC, Greene RW. 2012. CNS dopamine transmission mediated by noradrenergic innervation. J Neurosci. 32: 6072–6080.
Smith HR, Porrino LJ. 2008. The comparative distributions of the monoamine transporters in the rodent, monkey, and human amygdala. Brain Struct Funct. 213:73–91.
Smyser CD, Inder TE, Shimony JS, Hill JE, Degnan AJ, Snyder AZ, Neil JJ. 2010. Longitudinal analysis of neural network development in preterm infants. Cereb Cortex. 20:2852–2862.
Takahashi J, Shibata T, Sasaki M, Kudo M, Yanezawa H, Obara S, Kudo K, Ito K, Yamashita F, Terayama Y. 2015. Detection of changes in the locus coeruleus in patients with mild cognitive impairment and Alzheimer's disease: high-resolution fast spin-echo T_1-weighted imaging. Geriar Gerontol Int. 15 (3):334–340.
Taniwaki T, Okayama A, Yoshiura T, Togao O, Nakamura Y, Yamasaki T, Ogata K, Shigeto H, Ohyagi Y, Kira J, et al. 2007. Age-related alterations of the functional interactions within the basal ganglia and cerebellar motor loops in vivo. Neuroimage. 36:1263–1276.
Tomasi D, Volkow ND. 2014. Functional connectivity of substantia nigra and ventral tegmental area: maturation during adolescence and effects of ADHD. Cereb Cortex. 24:935–944.
Trillo L, Das D, Hsieh W, Medina B, Moghadam S, Lin B, Dang V, Sanchez MM, De Miguel Z, Ashford JW, et al. 2013. Ascending monoaminergic systems alterations in Alzheimer's disease. Translating basic science into clinical care. Neurosci Biobehav Rev. 37:1363–1379.
Tzourio-Mazoyer N, Landeau B, Papathanassiou D, Crivello F, Etard O, Delcroix N, Mazoyer B, Joliot M. 2002. Automated anatomical labeling of activations in SPM using a macroscopic anatomical parcellation of the MNI MRI single-subject brain. Neuroimage. 15:273–289.
Uddin LQ, Kelly AM, Biswal BB, Xavier Castellanos F, Milham MP. 2009. Functional connectivity of default mode network components: correlation, anticorrelation, and causality. Hum Brain Mapp. 30:625–637.
Van Dijk KR, Sabuncu MR, Buckner RL. 2012. The influence of head motion on intrinsic functional connectivity MRI. Neuroimage. 59:431–438.
Walsh JJ, Han MH. 2014. The heterogeneity of ventral tegmental area neurons: projection functions in a mood-related context. Neuroscience. 282C:101–108.
Weissenbacher A, Kasess C, Gerstl F, Lanzenberger R, Moser E, Windischberger C. 2009. Correlations and anticorrelations in resting-state functional connectivity MRI: a quantitative comparison of preprocessing strategies. Neuroimage. 47:1408–1416.

Wenk GL, Pierce DJ, Struble RG, Price DL, Cork LC. 1989. Age-related changes in multiple neurotransmitter systems in the monkey brain. Neurobiol Aging. 10:11–19.

Wilson AA, Johnson DP, Mozley D, Hussey D, Ginovart N, Nobrega J, Garcia A, Meyer J, Houle S. 2003. Synthesis and in vivo evaluation of novel radiotracers for the in vivo imaging of the norepinephrine transporter. Nucl Med Biol. 30:85–92.

Yoshimoto K, Yoshida T, Sorimachi Y, Hirano A, Takeuchi Y, Ueda S, Yasuhara M. 1998. Effects of age and ethanol on dopamine and serotonin release in the rat nucleus accumbens. Physiol Behav. 64:347–351.

Ystad M, Eichele T, Lundervold AJ, Lundervold A. 2010. Subcortical functional connectivity and verbal episodic memory in healthy elderly—a resting state fMRI study. Neuroimage. 52:379–388.

Zhang S, Ide JS, Li CS. 2012. Resting-state functional connectivity of the medial superior frontal cortex. Cereb Cortex. 22:99–111.

Zhang S, Li CS. 2010. A neural measure of behavioral engagement: task-residual low-frequency blood oxygenation level-dependent activity in the precuneus. Neuroimage. 49:1911–1918.

Zhang S, Li CS. 2014. Functional clustering of the human inferior parietal lobule by whole-brain connectivity mapping of resting-state functional magnetic resonance imaging signals. Brain Connectivity. 4:53–69.

Zhang S, Li CS. 2012a. Functional connectivity mapping of the human precuneus by resting state fMRI. Neuroimage. 59:3548–3562.

Zhang S, Li CS. 2012b. Functional networks for cognitive control in a stop signal task: independent component analysis. Hum Brain Mapp. 33:89–104.

Zhang S, Li CS. 2012c. Task-related, low-frequency task-residual, and resting state activity in the default mode network brain regions. Front Psychol. 3:172.

Zhang D, Snyder AZ, Fox MD, Sansbury MW, Shimony JS, Raichle ME. 2008. Intrinsic functional relations between human cerebral cortex and thalamus. J Neurophysiol. 100: 1740–1748.

Zhang D, Snyder AZ, Shimony JS, Fox MD, Raichle ME. 2010. Noninvasive functional and structural connectivity mapping of the human thalamocortical system. Cereb Cortex. 20:1187–1194.

Zuo XN, Di Martino A, Kelly C, Shehzad ZE, Gee DG, Klein DF, Castellanos FX, Biswal BB, Milham MP. 2010. The oscillating brain: complex and reliable. Neuroimage. 49:1432–1445.

Zuo XN, Kelly C, Adelstein JS, Klein DF, Castellanos FX, Milham MP. 2010. Reliable intrinsic connectivity networks: test-retest evaluation using ICA and dual regression approach. Neuroimage. 49:2163–2177.